Comparison study on the performance of two different gas-permeable membranes used in a membrane-aerated biofilm reactor

Yun Wu[a, b], Zuodong Wu[a, b], Hongliang Chu[d], Juan Li[a, b], Huu Hao NGO[c*], Wenshan Guo[c], Nan Zhang[d], Hongwei Zhang[a, b]

[a.] State Key Laboratory of Separation Membranes and Membrane Processes, Tianjin Polytechnic University, Tianjin 300387, China.

[b.] School of Environmental and Chemical Engineering, Tianjin Polytechnic University, Tianjin 300387, China

[c.] Centre for Technology in Water and Wastewater, School of Civil and Environmental Engineering, University of Technology Sydney, Broadway, NSW 2007, Australia

[d.] CNOOC Tianjin Chemical Research and Design Institute, Tianjin 300387, China

[*]Corresponding Author：

E-mail: ngohuuhao121@gmail.com; Tel.: +61-2-95142745

Abstract: This study compared the performance of two different gas-permeable membranes, PVDF and PP membrane, in a membrane-aerated biofilm reactor (MABR). The surface characteristics and membrane pore blocking of these two membrane materials were studied utilizing AFM, SEM and CLSM. The PVDF membrane surface was more rough and hydrophilic, and possessed a better microbial affinity compared to PP. Furthermore, the MABR equipped with a PVDF membrane removed more COD (97.06±0.97%) and TN (85.66±0.87%) compared to the MABR with PP membrane (87.13±0.87% and 71.13±0.71%, respectively). As well, the PP membrane exhibited severe membrane pore blocking and had a lower oxygen transfer rate than the PVDF membrane. It is concluded that the PVDF membrane has potential as an aeration membrane material for MABRs.

Keywords: Membrane-aerated Biofilm Reactor (MABR); Membrane Material; Membrane Surface Morphology; Oxygen Transfer Rate; Membrane Pore Blocking; Confocal Laser Scanning Microscope (CLSM)

1. Introduction

Nitrogen pollution in aquatic environment wastewater has become a very serious and widespread problem globally. In wastewater treatment plants, biological nitrogen removal processes are commonly used because they are economical and efficient [1]. Conventional biological nitrogen removal processes are usually conducted using at least two separate phases for aerobic nitrification and anoxic denitrification. This is a complicated operation where efficiency is poor in terms of oxygen and high energy

consumption [2, 3]. To overcome these problems, various systems have been developed to achieve simultaneous nitrification and denitrification (SND) in a single reactor, such as oxidation ditch, in a sequencing batch reactor. For example, Liu et al. [4] applied a Carrousel oxidation ditch to treat real domestic wastewater. The system achieved total nitrogen (TN) removal efficiency of 60–70% through SND, and NH_3–N and TN concentrations in effluent were less than 5 and 15 mg/L, respectively. In one study, Kulkarni [5] used a single sludge biomass system containing T. pantropha to remove nitrophenols by SND in SBRs. The removal rates were 97–99% for COD, 98% for 4-nitrophenol and 83–84% for 2,4-nitrophenol and 2,4,6-nitrophenol.

Furthermore, as a promising alternative option to conventional biofilm reactors, membrane-aerated biofilm reactors (MABRs) have been used for the treatment of various wastewaters through SND (e.g., ammonia wastewater [6], pharmaceutical wastewater [7], and landfill leachate [8, 9]). In MABR systems, the membrane not only serves as a biofilm carrier but also as an oxygen supply material. Close to the biofilm-membrane interface is the aerobic zone but this is low in organic substrate, while close to the biofilm-liquid interface is the anoxic zone which is high in organic substrate. It is well known that the nitrifying bacteria, including ammonia-oxidizing bacteria (AOB) and nitrite-oxidizing bacteria (NOB) are dominant in the rich aerobic zone, while denitrifying bacteria are dominant in the anoxic region [10]. Thus, SND can be achieved in a single MABR which provides a new symbiotic environment for aerobic and anaerobic microorganisms to remove nitrogen [11]. Moreover, due to its

non-bubble aeration and the multilayer structures of biofilm, MABRs have a better oxygen utilization and biodegradable ability than other conventional diffusion biofilm processes (e.g., biofilter, rotating biological contactor, biological contact oxidation) [12,13,14]. However, since the membrane is the carrier of the biofilm, and while the biofilm is growing the bacterial cells may gradually penetrate the membrane pores. This results in declining oxygen transfer and a change in the structure of the biofilm [15, 16]. Therefore, selecting an appropriate membrane is perhaps the most important approach when considering the MABR's performance [17].

Different materials and manufacturing technologies produce different membrane fibers in the surface morphology, pore characteristics and porosity [18]. The aeration membranes of MABRs should not only function well in terms of high oxygen transfer but also exhibit excellent pore blocking resistance and microbial affinity. According to the surface properties and structure of membrane materials, suitable membranes for MABRs include hydrophobic microporous membrane, dense membrane and composite membrane [19]. A dense membrane has a higher mass transfer resistance and may lead to less gas flux [20], while the production costs for making composite membranes are high and furthermore the manufacturing process is complicated [21]. Compared to the dense membrane and composite membrane, the hydrophobic microporous membrane has a higher gas flux and the price is moderate [22], which could be the first choice of researchers. Amongst the hydrophobic microporous membranes, polyvinylidene fluoride (PVDF) and polypropylene (PP) hollow fibers are the most commonly used

membranes in MABRs [23].

Wei, Xin et al. [24] designed a FT-MABR with a PP hollow fiber membrane as the aeration membrane to overcome the feed stream short-circuiting and achieve facilitated mass transfer. The TN removal efficiency reached 83.5% at the feed flow velocity of 0.05 m/s when the COD/N ratio was 7. Sun et al. [25] employed a PP membrane in a sequencing batch MABR and achieved nitrogen and phosphorus removal efficiently and simultaneously. The removal efficiencies of COD, NH_3–N, TN and TP were maintained above 90%, 96%, 91% and 85%, respectively. In other studies, researchers improved the performance of MABRs by modifying the surface of PVDF membrane fibers, for example by coating them with polyether-block-polyamide copolymer (PEBA) or L-3,4-dihydroxyphenylalanine (DOPA) [17,26]. However, detailed studies concerning the effects of their hydrophilic/hydrophobic properties, surface morphologies and biocompatibilities on the performance of MABRs are rare in the literature.

The purpose of this work is to investigate the effects of hydrophobic microporous PVDF and PP hollow fiber membranes on the performance of MABRs. With the help of atomic force microscopy (AFM) and scanning electron microscope (SEM), the performance of MABRs was investigated in terms of: (i) nitrogen and carbon removal; (ii) biomass property on membrane surface; and (iii) membrane pore blocking propensity. Furthermore, given the fact that there is no relatively perfect method to measure the membrane pore blocking in situ, this is the first time a confocal laser scanning microscope (CLSM) has been utilized to study the inner wall of aerated

membrane polluted by extracellular polymeric substances (EPS) and microorganisms during different operational phases. A preferable aeration membrane was selected for MABRs by comparing the performance of two materials in the MABR system. These are explained in more detail in the next section below.

2. Materials and methods

2.1 The MABR system

Two parallel MABRs set up with a working volume of 2.0 L and made of plexiglass are presented schematically in Fig. 1. Wastewater was supplied continuously using a peristaltic pump and the effluent was discharged through an overflow. As well, the reactor was designed with an inlet and an outlet to circulate water, and the circulation flow rate was controlled by a diaphragm pump. Air was supplied into the membrane lumen via a manifold using an air pump, the exhaust gas was emitted into the atmosphere through the other manifold. The experimental temperature was maintained at 25±0.5℃.

Fig. 1

The PVDF and PP hollow fiber membranes used in this study had pore sizes of 0.16 μm and 0.10 μm， and thicknesses of 0.15 mm and 0.08 mm, respectively. PVDF and PP membrane modules with the same fiber numbers and available length were installed into two stand-alone reactors (referred to as $R\text{-}_{PVDF}$ and $R\text{-}_{PP}$, respectively).

Moreover, the average contact angle values of PVDF and PP membrane fibers used in this study were 84.56° and 140.72°, respectively. Table 1 summarizes the characteristics of the membranes used in this analysis. In order to retain the same surface organic loading rates (11.58g COD/(m^2·d) and 2.32g NH_3-N/(m^2·d)), the influent flow rates were kept at 2.5 mL/min and 1.5 mL/min, and hydraulic retention times (HRT) were kept at 12h and 20h for R-$_{PVDF}$ and R-$_{PP}$, respectively. This is because the available membrane surface area was different.

Table 1. Characteristics of the membranes used in this study.

Description	***PVDF***	***PP***
Available membrane length (mm)	250.00	250.00
Membrane outer diameter (mm)	1.10	0.60
Membrane inner diameter (mm)	0.80	0.44
Membrane thickness (mm)	0.15	0.08
Membrane pore size (μm)	0.16	0.10
Bubble point (kPa)	25	0.3
The number of membrane fibers	100	100
Available membrane surface area (cm^2)	863.5	471.00
Contact angle (^{o})	84.56±1.69	140.72±2.81

2.2 Wastewater

Synthetic wastewater was used containing $C_6H_{12}O_6$ and NH_4Cl as the main sources of COD and NH_3-N with concentrations of 250±10 mg/L and 50±2 mg/L, respectively. Other components in the synthetic wastewater included KH_2PO_4 (10 mg/L), $CaCl_2·H_2O$ (10 mg/L), MgSO4·$7H_2O$ (10 mg/L), $FeSO_4·7H_2O$ (10 mg/L), $MnSO_4·H_2O$ (0.10 mg/L) [27]. Influent pH was kept between 7.8 and 8.3 by using $NaHCO_3$.

2.3 Reactor start-up and operation

The method of sludge recycling was used for biofilm formation in this study. The seeding sludge was taken from the secondary sedimentation tank of a Municipal Wastewater Treatment Plant (Tianjin, China) employing the A^2/O (anaerobic/anoxic/oxic) process. 4 h anaerobic cultivation and 12 h aerobic cultivation were done to obtain anaerobic/aerobic activated sludge for MABRs. Following inoculation, the sludge was added to MABRs with nutrients. During the recycling stage of the sludge, the wastewater was supplied continuously (2.5 mL/min for $R\text{-}_{PVDF}$ and 1.5 mL/min for $R\text{-}_{PP}$) and the recirculating flow rate was 7.50 mL/min. After 15 days, the sludge was discharged from the reactors once a biofilm was formed.

2.4 Analytical methods

2.4.1 Water quality analysis

Influent and effluent samples were filtered through a 0.45 μm filter paper (Millex Corp.) prior to analysis. COD, NH_4-N, NO_2-N, NO_3-N and T-N were measured accordingly using the Standard Methods (APHA, 1995). DO and pH were measured using a DO meter (LDO101, HACH) and pH meter (PHC101, HACH), respectively.

2.4.2 Membrane characterization

Two kinds of man-made membrane fibers (phase inversion method of manufacture method for PVDF and melt-spinning-cold stretching method for PP) are quite different in terms of appearance morphology, membrane pore characteristics and porosity,

resulting from their materials and manufacturing techniques. The surface roughness was examined using atomic force microscopy (AFM, 5500AFM/SPM, United States). Clean membrane fibers and used membrane fibers (with biofilm removed from the membrane fibers) were observed by scanning electron microscope (SEM, JEOLJSM-5600LV, Japan). Contact angle values were measured using a contact angle detector (YH-168A, Japan) with water as the detection liquid.

In addition, confocal laser scanning microscopy (CLSM) (Leica TCS SP8, Germany) was conducted to investigate the membrane pore blocking in situ. Fluorescein isothiocyanate (FITC, Sigma-Aldrich, United States), concanavalin A (Con A, Sigma-Aldrich, United States), calcofluor white (CW, Sigma-Aldrich, United States), STYO 63 (Molecular Probes, Thermo-Fisher) were used to identify proteins, α-polysaccharides, ß-D-glucopyranose polysaccharides cellulose and nucleic acid, respectively. The fluorescence of calcofluor white was detected via excitation at 400 nm and from the emission width at 410-480 nm (blue). The FITC probe was detected via excitation at 488 nm and emission at 500-540 nm (green). Excitation at 543 nm and emission at 550-600 nm were utilized to detect Con A conjugates. The fluorescence of SYTO 63 was determined on the basis of excitation at 633 nm and emission at 650-700 nm (red).

2.4.3 Microorganisms adhesion tests

Biomass of the biofilm on the membrane surface was calculated utilizing the gravimetric method [28]. For each measurement, triplicate samples (length: 3 cm) of

biomass were taken at the top, middle, and bottom of each membrane biofilm module and then suspended in 50 mL of demineralized water by a sonifier. This was followed by filtering through a 0.22 μm filter (GE Whatman Filter Paper) to obtain the average weight of the biomass. At the end of the experiment, vertical cross-sectional images of both PVDF and PP membrane fibers were taken by a high-resolution CCD camera (MLM3XMP-CCD, China) to measure the biofilm's thickness. The reported biofilm thickness was the mean of triplicate samples which were taken at the top, middle, and bottom of each membrane biofilm module.

2.4.4 Bubble point and Oxygen transfer study

Compared to conventional processes, the MABR has the specific advantage of high oxygen transfer efficiency due to its bubble-less aeration when the aeration pressure was below the membrane bubble point pressure. It is therefore necessary to measure the pressure of the membrane bubble point. Measuring the bubble point was done as follows: the membrane module was completely immersed in water with one end connected to an air pump and the other end sealed. Then the air pump was switched on to control the gas flow. The bubble point was the pressure in the membrane's inner lumen when the first bubble began to appear on the membrane's surface.

Oxygen transfer rate (OTR) is an important parameter for characterizing the ability to: firstly, supply oxygen through the membrane to the biofilm; and secondly, estimate the pore blocking of the membrane. The measurement method of oxygen transfer rate throughout the study was conducted as follows. Under the bubble point pressure of the

aeration membrane, the hollow fiber membrane module was connected to an air pump and immersed into distilled water in an airtight beaker of 2 L with a constant mechanical agitation. DO concentration of distilled water was monitored using a DO meter. Then, pure nitrogen gas was sparged into the airtight beaker to decrease DO concentration to 0 mg/L. After that the membrane aeration stage began by turning on the air pump. DO concentration was recorded as soon as it began to change as time passed. Once DO concentration in the bulk began to change linearly with time, the slope of the line was OTR (Fig. 2). With the surface area of about 863.5 and 471.0 cm^2, OTR values of clean PVDF and PP membrane modules were calculated as 1.126 ± 0.023g/d at the intermembrane pressure of 25kPa and 1.312±0.035g/d at 0.3kPa, respectively.

Fig. 2

3. Results and discussion

3.1 Performance of the two MABRs

The performance of the MABRs was evaluated with respect to COD and nitrogen removal efficiencies as presented in Figs. 3-5. As depicted in Fig. 3, respective COD removal efficiencies of these two reactors with the PVDF and PP membrane, were approximately 79.47% and 52.48% at the beginning of the experiment, then rose significantly to 94.92% and 84.56% within 20 days, reaching a plateau by day 70. After 70 days of operation the removal rate declined, and the COD removal efficiencies of the two reactors dropped to 90.22% and 77.14%, respectively, at the end of the experiment.

$R\text{-}_{PVDF}$ was about 12% higher than $R\text{-}_{PP}$ throughout the whole experimental process.

Fig. 3

Similar to COD removal, NH_3-N and TN removal efficiencies presented the same trends (Fig. 4 and Fig. 5). Figure 6 illustrates the composition of residual nitrogen compounds in the effluents. As can be seen from Fig. 6, NO_3-N in the effluents originating from the two reactors was accumulated within 35 days of operation, indicating that denitrification was limited in this period. The thin biofilms formed at the start-up stage transferred excess oxygen to the bulk liquid, which was favorable for nitrification using nitrifying bacteria. However, the high dissolved oxygen concentration limited the formation of an anaerobic zone on the biofilm's outer layer and the growth of denitrifying bacteria. This led to poor TN removal efficiencies which were only 35.84% for $R\text{-}_{PVDF}$ and 25.62% for $R\text{-}_{PP}$ at the beginning of the experiment. Until the 30^{th} day, the TN removal efficiency reached about 83.76% and 69.62% for $R\text{-}_{PVDF}$ and $R\text{-}_{PP}$, respectively, since a thick biofilm was observed.

The two reactors' NH_3-N removal efficiencies were 64.02% for $R\text{-}_{PVDF}$ and 57.53% for $R\text{-}_{PP}$, and then quickly increased to 94.97% and 87.91% in the first 20-day operation, respectively. At the same time, NO_2-N and NO_3-N were barely detected. However, the NH_3-N and T-N removal efficiencies of $R\text{-}_{PP}$ fell to 78.68% and 59.63% after day 70 while those of the $R\text{-}_{PVDF}$ were maintained at 96.40% and 82.66%, respectively. Therefore, the whole experimental period (90 days) could be divided into three phases

according to the curve of the removal rate for COD and nitrogen: phase I (0-30 days); phase II (31-65 days); and phase III (66-90 days). COD and nitrogen removal efficiencies changed during the operation as a consequence of the biofilm development. Superior performance of the R-$_{PVDF}$ than R-$_{PP}$ can be explained by different characteristics of the biofilm on the surface of different aeration membrane materials. Further details about this are discussed in Sections 3.2 and 3.3.

Fig. 4.

Fig. 5.

Fig. 6.

3.2 Characterization of membranes and biofilms in the two MABRs

It is well known that a biofilm's characteristics depend on the properties of the biocarrier's surface, flow velocity, dissolved oxygen and organic loading, etc. [29, 30]. The differences in biofilms created using a biocarrier can directly affect the performance of the two reactors. The surface morphology of the aeration membrane could have a critical impact on the development of the biofilm. To evaluate the membranes used in the MABR, three properties of the membrane need to be considered: surface roughness, OTR and contact angle. AFM was used to examine the roughness of the membrane surface [31]. As shown in Table 2, the arithmetic mean and root mean

square height of the clean PVDF membrane surface were (0.479 μm and 0.566 μm), which were triple the size of the clean PP membrane (0.148 μm and 0.172 μm), respectively. Thus, the surface of the clean PVDF membrane was rougher than that of the clean PP (Fig. 9).

Fig. 7.

Table 2. Evaluation parameters of membrane surface properties.

Description*	***PVDF***	***PP***
Sq (μm)	0.566	0.172
Ssk	0.317	0.067
Sku	2.05	1.89
Sp (μm)	1.46	0.359
Sv (μm)	1.22	0.349
Sz (μm)	2.68	0.707
Sa (μm)	0.479	0.148

*Sa, Arithmetic mean height; Sku, Kurtosis; Sp, Maximum peak height; Sq, Root mean square height; Ssk, Skewness; Sv, Maximum pit height; Sz, Maximum height

Additionally, microorganisms can adhere to the membrane easily by improving membrane hydrophilicity [32]. Oxygen concentration gradient can influence the growth of bacteria in the biofilm. Thus, the water contact angles and OTRs of membranes were measured to investigate the relationship between the development of biofilms and the surface properties of aeration membranes. In order to assess the properties of biofilms, a portion (length: 3 cm) of the fibers located at the middle section of the two membrane modules was selected to measure biomass (Table 3) based on the gravimetric method [28]. The biofilms were sampled when the removal efficiencies were relatively stable on

day 15 of phase I, day 45 of phase II and day 75 of phase III.

Table 3. Biomass on different membrane fibers.

Operation time (d)	*Biomass on PVDF membrane fibers (g·m^{-2})*	*Biomass on PP membrane fibers (g·m^{-2})*
15	17.85±0.25	13.37±0.15
45	23.98±0.58	18.82±0.41
75	26.34±0.62	21.46±0.50

The contact angle values and OTRs of the clean membrane surface suggest that the hydrophilicity of the PVDF membrane (contact angle 84.56°) was higher than that of the PP membrane (contact angle 140.72°), while the OTR of the PVDF membrane (1.126) was slightly lower than that of the PP membrane (1.312). Wilderer et al. [33] reported that the hydrophilicity of the membrane surface benefits the growth of the biofilm and reduction of the microbial domestication period. Therefore, the PVDF membrane fibers with a rough and hydrophilic surface and a high OTR which could accelerate biofilm formation were more prone to being adhered by microorganisms. As can be seen from Table 3, the biofilms attached onto the PVDF and PP membrane fibers grew well in phase I, which were 17.85 g/m^2 and 13.37 g/m^2 (on day 15), respectively.

Furthermore, the MABR is a counter-diffusion system of oxygen and substrates. The NH_3-N and COD spread from the biofilm's outer surface to the inner surface, while oxygen permeated exactly in the opposite direction through the biofilm layer. Kazuaki Hibiya et al. [34] reported DO concentration in the MABRs was maintained at 0.5 mg/L. The outer layer of biofilm was in a hypoxic environment, which is suitable for

denitrifying bacteria; meanwhile nitrifying bacteria near the membrane lumen maintained a high nitrification rate with plenty of oxygen. The distributions of nitrifying bacteria and denitrifying bacteria will be affected by the thickness of biofilm and oxygen concentration gradient from the membrane surface to the biofilm surface.

Therefore, in phase II, biomass accumulated up to 23.98 g/m^2 and 18.82 g/m^2 (on day 45) on PVDF and PP membranes at a high rate of 0.21 $g/(m^2 \cdot d)$ and 0.18 $g/ (m^2 \cdot d)$, respectively. An increase in the biomass indicated the following: a well-established activity of nitrifying bacteria and denitrifying bacteria and the maturity of biofilm [35]. The concentrations of NO_2-N and NO_3-N in the effluents of two reactors were maintained at low levels and NH_4-N and TN removal efficiencies were maintained at quite high values (Fig. 6), suggesting that the anoxic and aerobic zones were formed in the biofilm which could be conducive for SND [36]. However, compared with phase II, the biomass growth increased slowly (0.08 $g/ (m^2 \cdot d)$ on PVDF membrane fibers and 0.09 $g/ (m^2 \cdot d)$ on PP, respectively) in phase III. This meant that the biofilm might decay and detach from the membrane surface as the OTR decreased dramatically (Table 4). On day 75, biomass on PVDF and PP membrane fibers increased up to 26.34 g/m^2 and 21.46 g/m^2, respectively, and the growth rate in phase III was about 50% less than phase II.

Fig. 8

In order to calculate the biofilm's thickness and density, vertical cross-sectional

images of clean membrane fibers and used membrane fibers with biofilms at the end of the experiment were taken using a CCD camera. As shown in Fig. 8, the diameters of clean PVDF and PP membrane fibers were 1.10 mm and 0.60 mm, respectively. The thickness of the biofilm on the PP membrane fiber was thinner (0.45±0.02 mm) than that of the PVDF membrane fiber (0.80±0.04 mm). However, the biofilm density of the PP membrane fiber (0.023g/cm^3) was higher than that of the PVDF membrane fiber (0.019g/cm^3). It was discovered that when oxygen and organics diffused into the biofilm in an opposite direction a certain concentration gradient could be established [37].

In work conducted by La et al. [38], with the increasing density of biofilm, the diffusion coefficient of oxygen and substrate decreased, which in turn reduced the substrate's penetration of the biofilm. Consequently, this brought about detachment and self-digestion of bacteria in the biofilm, and released more extracellular polymeric substances (EPS) which consisted of polysaccharides, proteins, lipids, nucleic acids, etc. The organic matter accumulated on the biofilm-membrane interface would permeate into membrane pores and be adsorbed on the pore walls [39]. This consequently led to two things: firstly, membrane pore blocking occurring; and a decline in the performance of the MABRs in phase III (Figs. 3-5). Overall, the MABR with PVDF membrane in this study could maintain appropriate thickness of biofilm, SND efficiency and stable removal rate of COD and nitrogen. Furthermore, the performance of R-$_{PVDF}$ was superior to that of R-$_{PP}$ throughout the whole experimental process.

3.3 OTR performance of the two MABRs

The microporous structure and characteristics of the hollow fiber membranes are different in terms of the membrane preparation methods utilized [40]. The most commonly used preparation technique for PVDF hollow fiber membrane is the phase inversion method while that for manufacturing PP membranes is the melt-spinning-cold stretching method (MSCS) [41]. The PVDF membranes prepared with the phase inversion method are asymmetric membranes possessing a sponge-type or finger-type structure with a dense skin at the surface [42]. The PP membranes prepared by the MSCS method have a relatively uniform pore size distribution with parallel pores penetrating the entire membrane cross-section [43]. Therefore, the bubble point pressure of the PP membrane (0.3kPa) is much lower than that of the PVDF membrane (25kPa), while the OTR of the PP membrane is higher than that of the PVDF membrane. If membrane pores are blocked throughout the experiment, the OTR will decline and adversely affect the performance of the MABRs. As Sections 3.1 and 3.2 noted, both the performance of the MABRs and OTR gradually declined periodically, demonstrating that the membrane pores were blocked. To obtain detailed information about pore blocking, SEM and CLSM analyses were carried out to compare morphological changes between clean and used membranes. The OTR and contact angle of membrane lumen were measured at each experimental phase (Table 4) to investigate the change in membrane properties. Before the analysis, the biofilm was removed from

the membrane surface via a soft brush in distilled water without changing the membrane's surface morphology.

Table 4. The OTR and Contact angle of membrane lumen of the two reactors in different phases

Operation time (d)	R_{PVDF}			R_{PP}		
	15th day	*45th day*	*75th day*	*15th day*	*45th day*	*75th day*
Oxygen transfer rate（g/d)	1.075 ±0.05	0.994 ±0.04	0.720 ±0.03	1.113 ±0.06	0.827 ±0.04	0.582 ±0.03
contact angle (°)	83.78 ±1.55	81.83 ±1.50	78.96 ±1.45	124.43 ±2.35	116.64 ±2.10	106.47 ±2.00

Fig. 9

Figure 9 presents the SEM images of membrane fibers. There were significant differences of surface morphology between two types of clean membranes, as well as the used membranes. It is shown in Fig. 9(a) and (c) that the PP membrane had a larger number of pores per surface area than the PVDF membrane, and the surface of the PVDF membrane was uneven with an imbricated texture while the surface of the PP membrane was smooth with uniform pores. Comparing Fig. 9(b) and (d), the pores on the PP membrane surface were totally covered by foulants which were denser compared to those on the PVDF membrane in contrast to the SEM images of clean membrane fibers. Based on the above analysis of the membrane performance and SEM results, it can be concluded that the PVDF membrane demonstrated better resistance to pore blocking than the PP membrane.

In order to verify this assumption, the membrane pores' interior needs to be explored in situ. It is reported that fluorescently labeled lectins represent one of the best

approaches for the investigation of biofilms in situ [44]. The multicolor fluorescence labeling could provide information on the detailed architecture and distribution of EPS and metabolites of biofilms in membrane pores. Chen et al. [45] investigated the distributions of cells (nucleic acids) and EPS (proteins, α- and ß-D-glucopyranose polysaccharides) in the fouling layer on a filter membrane. This study applied the CLSM technique to assess the membrane pores and stained the sample according to the method employed by Chen [45].

Fig. 10

Fig. 10 presents the CLSM images of membrane fibers in different operation phases which could differentiate foulants that induce membrane pore blocking by using different fluorochrome to identify the components. The fluorescent displays of red, green and blue indicate there are existing cells (SYTO 63, red), polysaccharides (Con A, light blue), and proteins (FITC, green) in the membrane pores. Comparing the six pictures in Fig. 10, in phase I (Fig. 10 (a) (d)), there is no fluorescence on PVDF and PP membranes due to fewer microorganisms attaching to the membrane surface. In phase II (Fig. 10 (b) (e)), the biofilm was matured and developed. Under the suitable scenario of oxygen and organic substrate concentration, less EPS was released from the bacteria in the biofilm. There was a sprinkling of red and green fluorescence due to the pore size distribution (caused by membrane preparation methods) that was blocked by EPS.

With the development of a matured biofilm and decrease in diffusion coefficients

of oxygen and substrate, the bacteria decayed and released more EPS to accumulate on the biofilm-membrane interface. As the experiment proceeded, the EPS would permeate into membrane pores and be adsorbed on the walls of the pores. These substances would make the pore walls wet, transforming pores from hydrophobic to hydrophilic, which could help liquids penetrate the pores and aggravate membrane pore blocking [46]. Table 4 shows that the contact angle value of membrane lumen gradually declined periodically as well as OTR, especially the PP membrane after day 45. The strong fluorescence reaction as shown in Fig.10(c and f) precisely confirmed that the membrane pores were blocked, and the two reactors' performance began to falter after 65 days in phase III. As well, the more hydrophilic the membrane was, the higher the adsorption equilibrium constant would be [47]. This indicated that the pollutants on the membrane had greater dynamic adsorption capacity. Furthermore, as the pores of the PP membrane penetrated the entire membrane cross-section, the pollutants were more easily permeated into the inner surfaces and soaked the membrane pore, which obstructed the diffusion of oxygen from the inner surface of the membrane to the biofilm. Therefore, the contact angle and ORT values of the PP membrane declined more quickly than those of the PVDF membrane as shown in Table 4.

4. Conclusion

It can be summarized that the PVDF membrane was more favorable for the attachment of microorganisms than the PP membrane due to the surface roughness. The

hydrophilicity of the PVDF membrane was higher than that of the PP membrane. In addition, the PVDF membrane with an asymmetric pore structure and this indicated better resistance to membrane pore blocking. Subsequently, the MABR with PVDF membrane proved to be more efficient and stable in performance than the PP membrane, specifically regarding the removals of organic material, nitrogen and OTR. Overall, compared to the PP membrane, the PVDF membrane was more suitable for utilization in MABRs.

Acknowledgements

This work was financially supported by the National Natural Science Foundation of China (No. 51678410, No. 51878448), and Key Projects of National Natural Science Foundation of China (No. 51638011). The authors are also grateful for the research collaboration between Tianjin Polytechnic University and University of Technology Sydney, especially on the Opening Research Fund of State Key Laboratory of Hollow Fiber Membrane Materials and Processes.

References

[1] Downing, L. S., Nerenberg, R., Total nitrogen removal in a hybrid, membrane-aerated activated sludge process, Water Research 42 (2008): 3697-3708.

[2] Semmens, M. J., et al., COD and nitrogen removal by biofilms growing on gas permeable membranes, Water Research 37.18 (2003): 4343-4350.

[3] Zhang, Tian Cheng, Y. C. Fu, Bishop, P.L., Competition for Substrate and Space in Biofilms, Water Environment Research 67.6 (1995): 992-1003.

[4] Liu, Y., et al., Study of operational conditions of simultaneous nitrification and denitrification in a Carrousel oxidation ditch for domestic wastewater treatment, Bioresource Technology 101.3 (2010): 901-6.

[5] Kulkarni, Pradnya, Nitrophenol removal by simultaneous nitrification denitrification (SND) using T. pantotropha, in sequencing batch reactors (SBR), Bioresource Technology 128.1 (2013): 273-280.

[6] Lin, J. Y., Zhang, P. Y., Yin, J., et al., Nitrogen removal performances of a polyvinylidene fluoride membrane-aerated biofilm reactor, International Biodeterioration & Biodegradation 102 (2015): 49-55.

[7] Lai, P., Chen, X. M., Yu, Y. F., et al., Biodegradation of pharmaceuticals in membrane aerated biofilm reactor for autotrophic nitrogen removal: A model-based evaluation, Journal of Membrane Science 494 (2015): 39-47.

[8] Syron, E., Semmens, M. J., Casey, E., Performance analysis of a pilot-scale membrane aerated biofilm reactor for the treatment of landfill leachate, Chemical Engineering Journal 273 (2015): 120-129.

[9] Syron, E., Casey, E., Membrane-aerated biofilm for high rate biotreatment: performance appraisal, engineering principles, scale-up, and development requirement, Environmental Science & Technology 42 (2008): 1833-1844.

[10] Susanne, L., Akihiko, T., Mogens, H., et al., Nitritation performance in

membrane-aerated biofilm reactors differs from conventional biofilm systems, Water Research 44 (2010): 6073-6084.

[11] Ni, B. J., Yuan, Z., A model-based assessment of nitric oxide and nitrous oxide production in membrane-aerated autotrophic nitrogen removal biofilm systems, Journal of Membrane Science 428 (2013): 163-171.

[12] Terada, A., Hibiya, K., Nagai, J., et al., Nitrogen removal characteristics and biofilm analysis of a membrane-aerated biofilm reactor applicable to high-strength nitrogenous wastewater treatment, Journal of Bioscience & Bioengineering 95 (2003): 170-178.

[13] Jie, W., Fanghua, B., Huu-Hao, N., Wenshan, G., Hui, J., Hongwei, Z., Xinbo, Z. 2016. Evaluation of energy-distribution of a hybrid microbial fuel cell-membrane bioreactor (MFC-MBR) for cost-effective wastewater treatment. Bioresource Technology 200(2016):420-425.

[14] Khaisri, Sakarin, et al. Comparing membrane resistance and absorption performance of three different membranes in a gas absorption membrane contactor, Separation & Purification Technology 65.3 (2009): 290-297.

[15] Rothemund, C., Camper, A., Biofilms growing on gas permeable membranes, Water Science & Technology 29 (1994): 447-454.

[16] Semmens, M. J., Shanahan, J. W., Influence of a nitrifying biofilm on local oxygen fluxes across a micro-porous flat sheet membrane, Journal of Membrane Science 277 (2006): 65-74.

[17] Hou, F., et al., Surface modification of PVDF hollow fiber membrane and its application in membrane aerated biofilm reactor (MABR), Bioresource Technology 140.3 (2013): 1-9.

[18] Wu, Y., Zhang, N., Zhang, H.W., et al., CFD stimulation of internal hydrodynamic characteristics and optimization of membrane module in membrane aerated biofilm reactor, Journal of Chemical Industry & Engineering (China) 66 (2015): 402-409.

[19] Syron, Eoin, Casey, E., Membrane-Aerated Biofilms for High Rate Biotreatment: Performance Appraisal, Engineering Principles, Scale-up, and Development Requirements, Environmental Science & Technology 42.6 (2008): 1833-44.

[20] Zhang, Y., Li, T.G., Qiang, Z.M., et al., Current research progress on the membrane-aerated biofilm reactor, Acta Scientiae Circumstantiae (China) 31 (2011): 1133-1143.

[21] Terada, A., Yamamoto, T., Hibiya, K., et al., Enhancement of biofilm formation onto surface-modified hollow-fiber membranes and its application to a membrane-aerated biofilm reactor, Water Science & Technology 49 (2004): 263-268.

[22] Martin, K.J., Nerenberg, R., The membrane biofilm reactor (MBfR) for water and wastewater treatment: Principles, applications, and recent developments, Bioresource Technology 122 (2012): 83-94.

[23] Atchariyawut, Supakorn, et al., Effect of membrane structure on mass-transfer in the membrane gas–liquid contacting process using microporous PVDF hollow fibers, Journal of Membrane Science 285.1–2 (2006): 272-281.

[24] Wei, Xin, et al., COD and nitrogen removal in facilitated transfer membrane-aerated biofilm reactor (FT-MABR), Journal of Membrane Science 389 (2012): 257-264.

[25] Sun, Linquan, et al., Enhanced biological nitrogen and phosphorus removal using sequencing batch membrane-aerated biofilm reactor, Chemical Engineering Science 135 (2015): 559-565.

[26] Nisola, G. M., Orata-Flor, J., Oh, S., et al., Partial nitrification in a membrane-aerated biofilm reactor with composite PEBA/PVDF hollow fibers, Desalination & Water Treatment 51 (2013): 5275-5282.

[27] Syron, E., Casey, E., Model-based comparative performance analysis of membrane aerated biofilm reactor configurations, Biotechnology & Bioengineering 99 (2008): 1361-1373.

[28] Trulear, Michael G., and Characklis, W.G., Dynamics of Biofilm Processes, Journal 54.9 (1982): 1288-1301.

[29] Jia, H., Yang, G., Wang, J., Ngo, H.H., Guo, W., Zhang, H., Zhang, X., Performance of a microbial fuel cell-based biosensor for online monitoring in an integrated system combining microbial fuel cell and upflow anaerobic sludge bed reactor. Bioresource Technology218（2016）, 286-293.

[30] Casey, E. Glennon, B., Hamer, G., Biofilm development in a membrane-aerated biofilm reactor: effect of flow velocity on performance, Biotechnology & Bioengineering 67.4 (2000): 476-486.

[31] Gao, F., Wang, J., Zhang, H., Jia, H., Cui, Z., Yang, G., Role of ionic strength on protein fouling during ultrafiltration by synchronized UV-vis spectroscopy and electrochemical impedance spectroscopy. Journal of Membrane Science563(2018), 592-601.

[32] Rana, D., Matsuura, T., Surface modifications for antifouling membranes, Chemical Review 110 (2010): 2448-2471.

[33] Characklis, W.G., Wilderer, P.A., Structure and function of biofilms. John Wiley & Sons, 1989.

[34] Hibiya, K., Terada, A., Tsuneda, S., Hirata, A., Simultaneous nitrification and denitrification by controlling vertical and horizontal microenvironment in a membrane-aerated biofilm reactor, Biotechnology 100 (2002): 23-32.

[35] Pelicer-Nacher, C., Smets, B. F., Structure, composition, and strength of nitrifying membrane-aerated biofilms, Water Research, 57 (2014): 151-161.

[36] Wang, B., He, S., Wang, L., et al., Simultaneous nitrification and denitrification in MBR, Water Science & Technology 52 (2005): 453-442.

[37] Siegrist, H., Gujer, W., Mass transfer mechanisms in a heterotrophic biofilm, Water Research19 (1985): 1369-1378.

[38] La Motta, E. J., Internal diffusion and reaction in biological films, Environmental Science & Technology 10 (1976): 765-769.

[39] Wang, J., Zheng, Y., Jia, H., Zhang, H., Bioelectricity generation in an integrated system combining microbial fuel cell and tubular membrane reactor: Effects of

operation parameters performing a microbial fuel cell-based biosensor for tubular membrane bioreactor. Bioresource Technology170(2014), 483-490.

[40]Gerlach, K., Kessler, E., Methods for the preparation of porous fibers and membranes, US Patent No. 4564488, 1986-01-14.

[41] Mulder, Marcel, Basic Principles of Membrane Technology, Zeitschrift Für Physikalische Chemie 203.Part_1_2 (1998): 263-263.

[42] Rajabzadeh, Saeid, et al., Preparation of PVDF hollow fiber membrane from a ternary polymer/solvent/nonsolvent system via thermally induced phase separation (TIPS) method, Separation & Purification Technology 63.2 (2008): 415-423.

[43] Samuels, R.J., High strength elastic polypropylene, Journal of Polymer Science, Polymer Physics Edition 17. 4 (1979): 535－568.

[44] Flemming, H.C., Neu, T.R., Wozniak, D.J., The EPS matrix: the "house of biofilm cells", Journal of Bacteriology 189.22 (2007): 7945-7947.

[45] Chen, Ming Yuan, et al., Fluorescent staining for study of extracellular polymeric substances in membrane biofouling layers, Environmental Science & Technology 40.21 (2006): 6642-6646.

[46] Reij, Martine W., Keurentjes, J.T.F., and S. Hartmans, S., Membrane bioreactors for waste gas treatment, Journal of Biotechnology 59.3 (1998): 155-167.

[47] Xiao, Kang, et al., Combined effect of membrane and foulant hydrophobicity and surface charge on adsorptive fouling during microfiltration, Journal of Membrane Science 373.1 (2011): 140-151.

Figure captions

Fig.1. Schematic diagram of the MABR

Fig. 2. Oxygen transfer rate for different membrane module

Fig. 3. COD removal efficiency of two MABRs with different membrane materials

Fig. 4. NH_3-N removal efficiency of two MABRs with different membrane materials

Fig. 5. TN removal efficiency of two MABRs with different membrane materials

Fig. 6. Concentration variations of NO_2^--N and NO_3^--N in the effluents of two MABRs with different membrane materials

Fig. 7. AFM surface topographies of the membrane fibers: clean PVDF membrane (A); clean PP membrane (B). (Scan area: 5.0μm ×5.0μm)

Fig. 8. Images of different membrane fibers in vertical section: (a) clean PVDF membrane fiber; (b) used PVDF membrane fiber at75th day; (c) clean PP membrane fiber; (d) used PP membrane fiber at 75th day

Fig. 9. SEM images of membrane fibers: (a) clean PVDF membrane; (b) used PVDF membrane without biofilms; (c) clean PP membrane; (d) used PP membrane without biofilms.

Fig. 10. CLSM images of inner surface of membrane fibers: (a)-(c) for phase I (15th day), phase II (45th day) and phase III (75th day) of PVDF membrane fibers, respectively; (d)-(f) for phase I (15thday), phase II (45th day) and phase III (75th day) of PP membrane fibers, respectively. (Proteins (FITC), green; α-polysaccharides (Con A), light blue; cellulose (CW), blue; total cells (SYTO 63), red .)

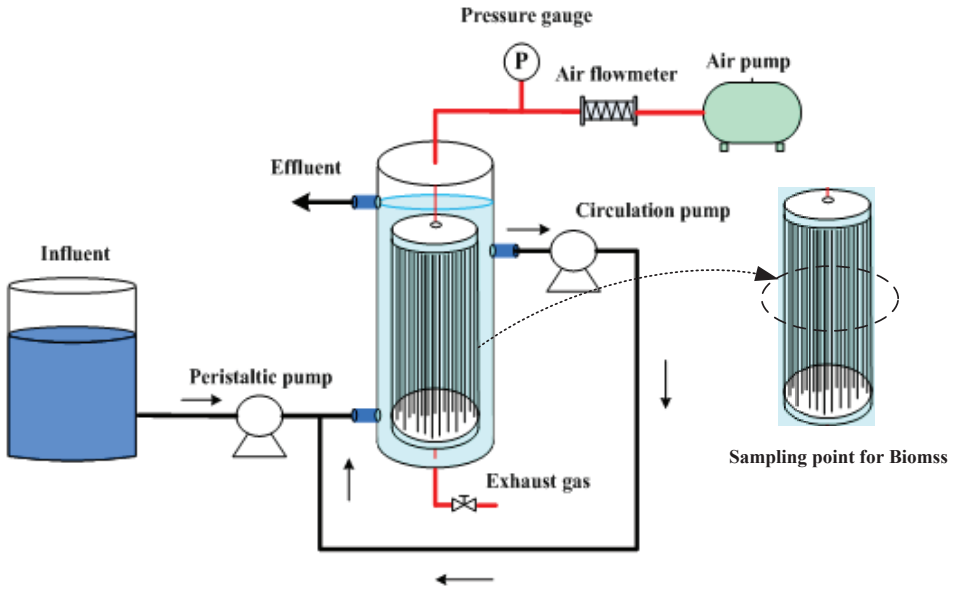

Fig.1

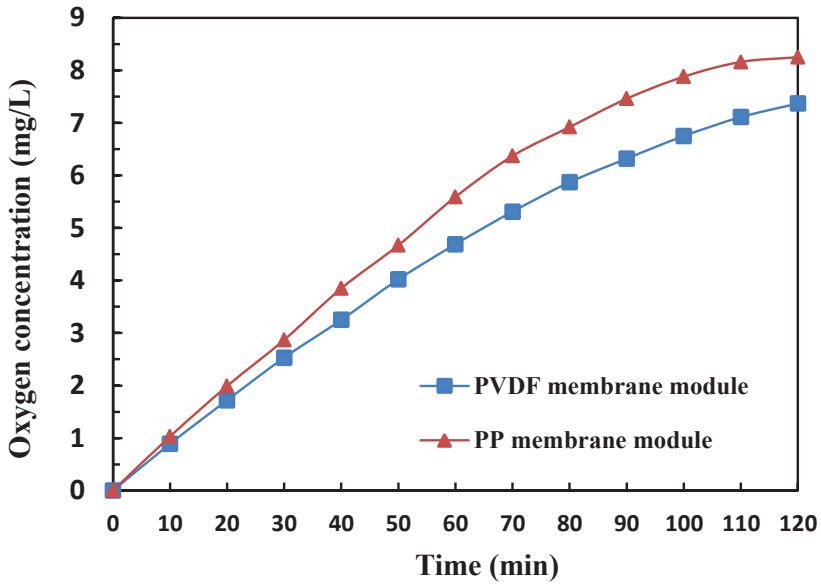

Fig. 2

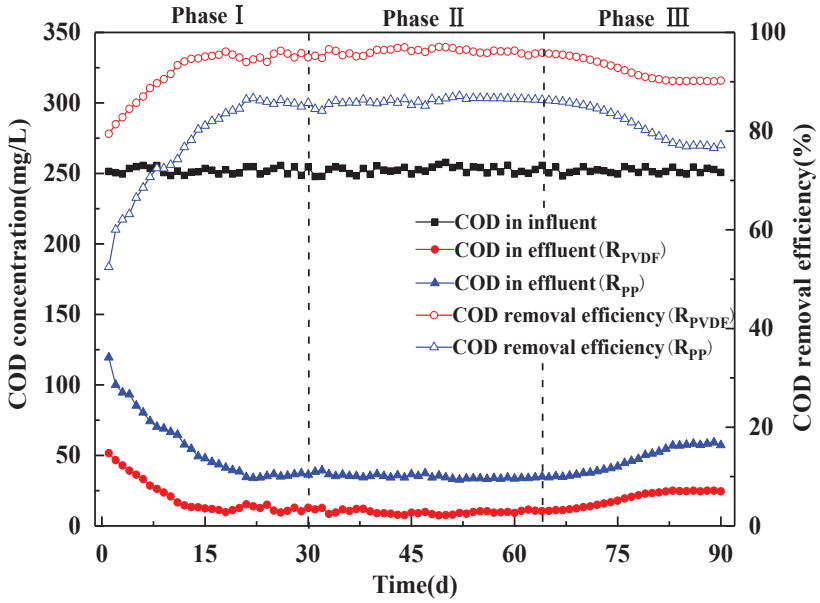

Fig. 3

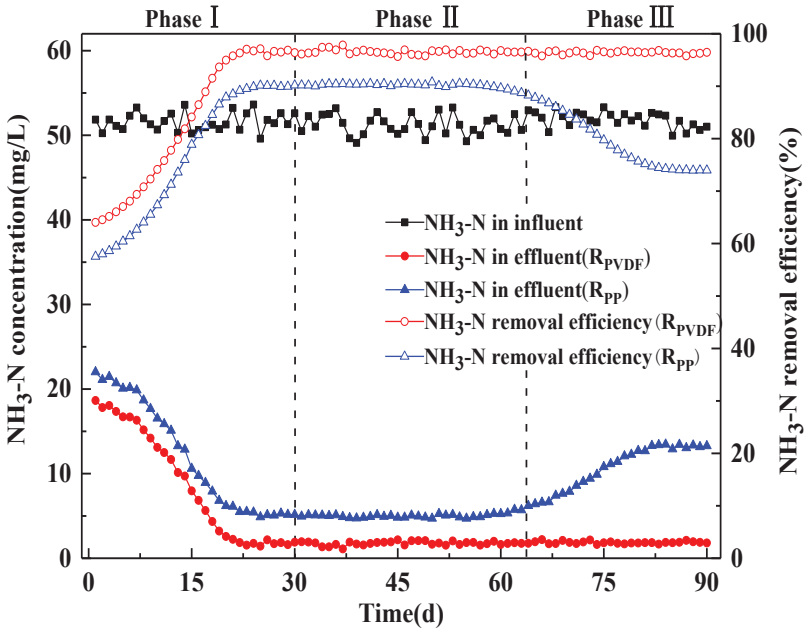

Fig. 4

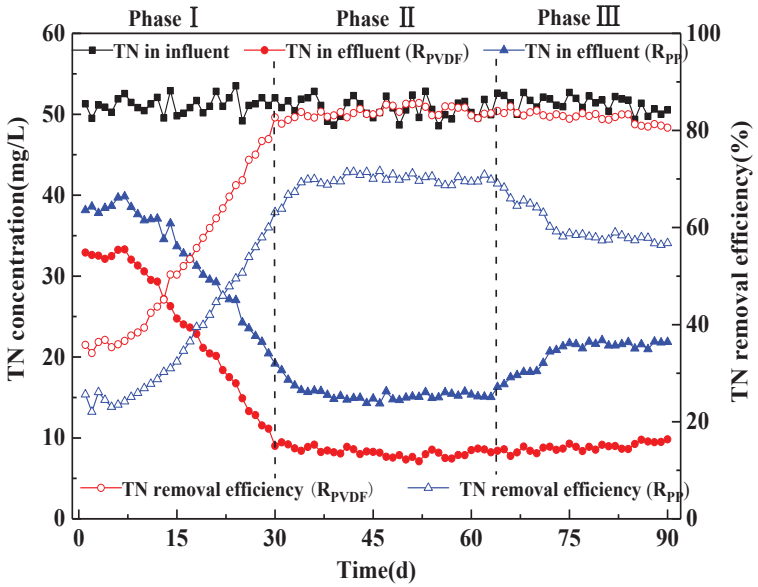

Fig. 5

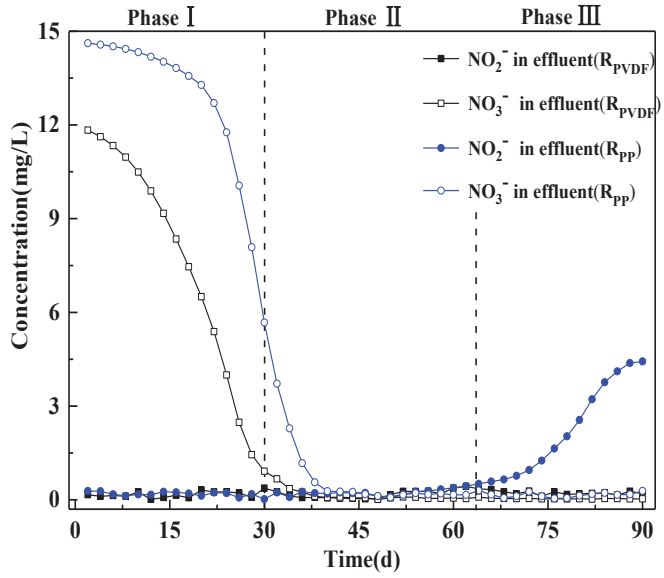

Fig. 6

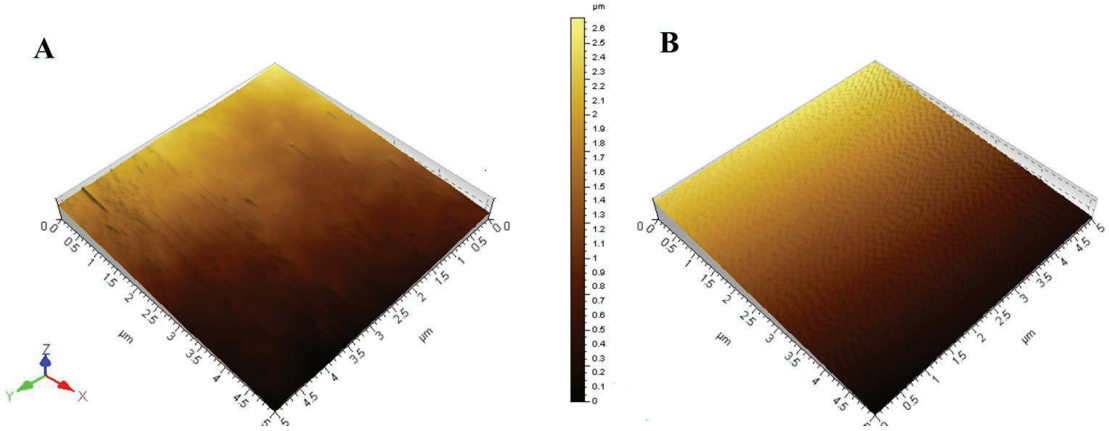

Fig. 7

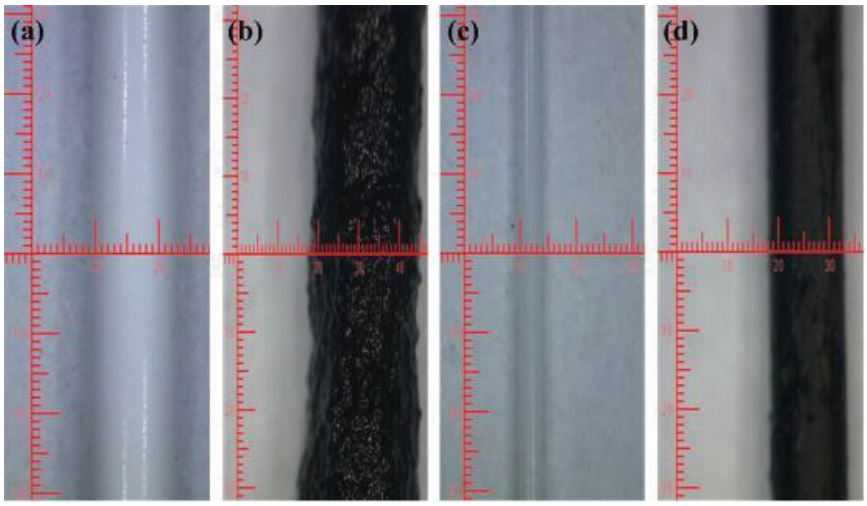

Fig. 8

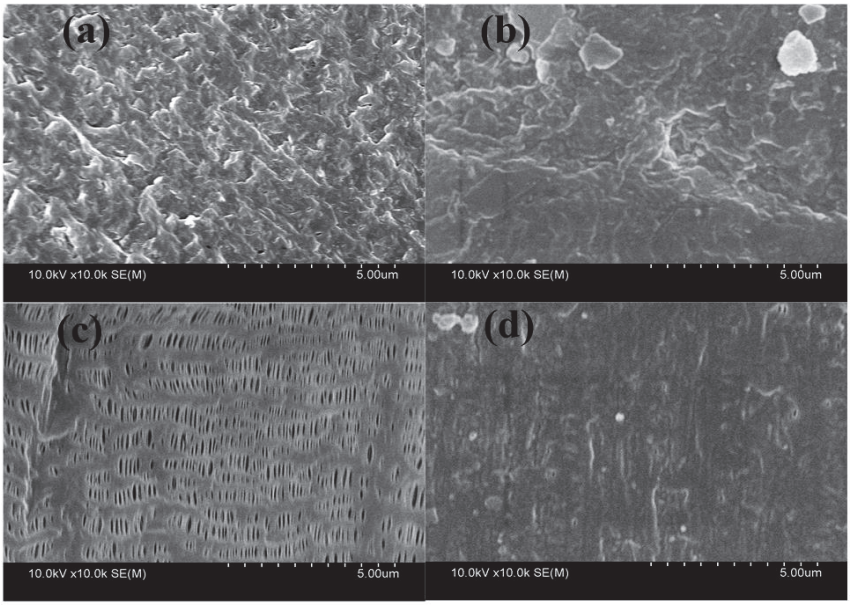

Fig. 9

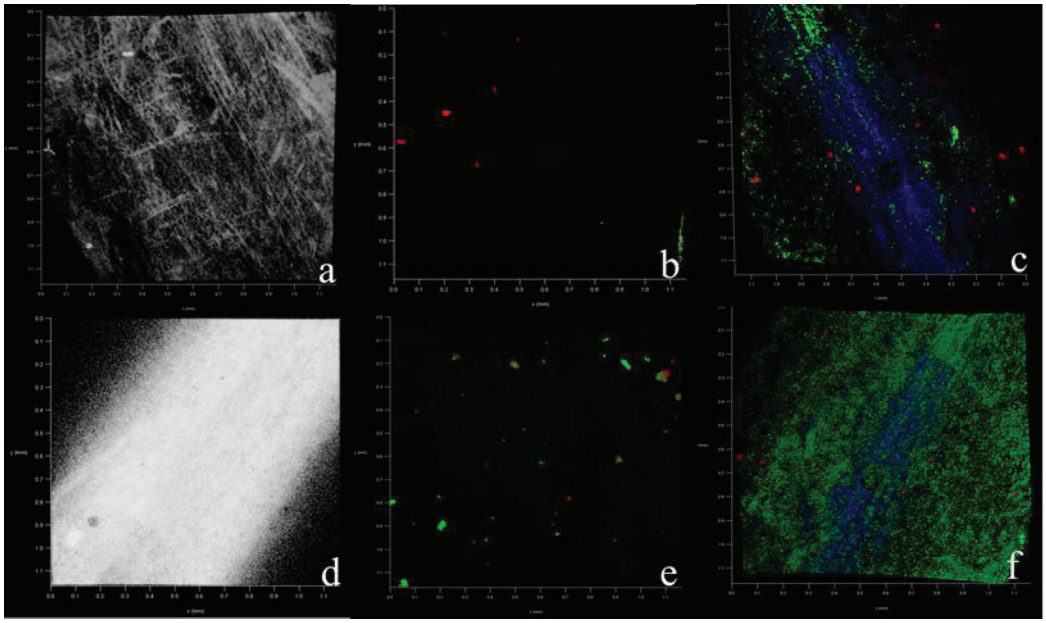

Fig. 10